

# Constraining new physics with collider measurements of Standard Model signatures

Jonathan M. Butterworth<sup>1</sup>, David Grellscheid<sup>2</sup>,  
Michael Krämer<sup>3</sup>, Björn Sarrazin<sup>3</sup>, David Yallup<sup>1</sup>

<sup>1</sup>*Department of Physics and Astronomy, University College London,  
Gower St., London, WC1E 6BT, UK*

<sup>2</sup>*IPPP, Department of Physics,  
Durham University, DH1 3LE, UK*

<sup>3</sup>*Institute for Theoretical Particle Physics and Cosmology,  
RWTH Aachen University, 52056 Aachen, Germany*

May 24, 2018

## Abstract

A new method providing general consistency constraints for Beyond-the-Standard-Model (BSM) theories, using measurements at particle colliders, is presented. The method, ‘Constraints On New Theories Using Rivet’, CONTUR, exploits the fact that particle-level differential measurements made in fiducial regions of phase-space have a high degree of model-independence. These measurements can therefore be compared to BSM physics implemented in Monte Carlo generators in a very generic way, allowing a wider array of final states to be considered than is typically the case. The CONTUR approach should be seen as complementary to the discovery potential of direct searches, being designed to eliminate inconsistent BSM proposals in a context where many (but perhaps not all) measurements are consistent with the Standard Model. We demonstrate, using a competitive simplified dark matter model, the power of this approach. The CONTUR method is highly scaleable to other models and future measurements.

IPPP-16-52, MCNET-16-21, TTK-16-22

## 1 Introduction

The Large Hadron Collider (LHC) is probing physics in a new kinematic region, at energies around and above the electroweak symmetry-breaking scale. With the discovery of the Higgs boson [1,2], the first data-taking period of the LHC experiments demonstrated that the understanding of electroweak symmetry-breaking within the Standard Model (SM) is broadly correct, and thus that the theory is potentially valid well above the TeV scale. Many precision measurements of jets, charged leptons, and other final states have been published, reaching into this new kinematic domain. The predictions of the SM are generally in agreement with the data, while the many dedicated searches for physics beyond the SM have excluded a wide range of possible scenarios. Nevertheless, there are many reasons to be confident that physics beyond the Standard Model (BSM) exists; examples include the gravitational evidence for dark matter, the large preponderance of matter over antimatter in the universe, and the existence of gravity itself. None of these can be easily accommodated within known Standard Model phenomenology.

This motivates a continued campaign to make precise measurements and calculations at higher energies and luminosities, and to exploit these measurements to narrow down the class of viable models of new physics, hopefully shedding light on the correct new theory, or at least on the energy scale at which new physics might be observed at future experiments. Whether physics beyond the Standard Model is discovered or not, there is a need to extract the clearest and most generic information about physics in this new energy regime, an imperative which will grow with integrated luminosity.

In this paper we exploit three important developments to survey existing measurements and set limits on new physics.

1. SM predictions for differential and exclusive, or semi-exclusive, final states are made using sophisticated calculational software, often embedded in Monte Carlo generators capable of simulating full, realistic final states [3]. These generators now incorporate matrix-elements for higher-order processes matched to logarithmic parton showers, and successful models of soft physics such as hadronisation and the underlying event. They are also capable of importing new physics models into this framework, thus allowing the rapid prediction of their impact on a wide variety of final states simultaneously. In this paper we make extensive use of these capabilities within Herwig 7 [4, 5].
2. As the search for many of the favoured BSM scenarios has been unsuccessful, there has been a move toward “simplified models” of new physics [6, 7], which aim to be as generic as possible and which provide a framework for interpreting BSM signatures with a minimal amount of new particles, interactions and model assumptions. The philosophy is similar to an “effective lagrangian” approach in which effective anomalous couplings are introduced to describe new physics, but is more powerful, as such simplified models also include new particles, and thus can remain useful up to and beyond the scale of new physics — a region potentially probed by LHC measurements.
3. The precision measurements from the LHC have mostly been made in a manner which minimises their model-dependence. That is, they are defined in terms of final-state signatures in fiducial regions well-matched to the acceptance of the detector. Many such measurements are readily available for analysis and comparison in the Rivet library [8].

These three developments together make it possible to efficiently bring the power of a very wide range of data to bear on the search for new physics. While such a generic approach is unlikely to compete in terms of speed and sensitivity with a search optimised for a specific theory, the breadth of potential signatures and models which can be covered makes it a powerful complementary approach.<sup>1</sup> On the one hand, any theory seeking to explain a new signature or anomaly in the data may predict a BSM signal in other final states, which should be checked against data this way. On the other hand, if no BSM physics emerges, a model-independent and systematic approach becomes mandatory to exclude new physics models or narrow down the corresponding model parameter space.

In this paper, we first motivate and describe the simplified model we have chosen as an initial demonstration, and the tools we use for its simulation. In Section 3 we introduce the measurements that we will use, and their implementation in Rivet. Section 4 covers the core of the CONTUR method, including the statistical approach and dynamic data selection and the assumptions made in this initial study. In Section 5 we discuss the differential cross sections in which the impact of our example model would be most apparent. In Section 6 this impact is translated into limits on the model parameters, and this is followed by our conclusions.

## 2 Simplified Model

Searches for new physics at the LHC are often interpreted in terms of simplified models. Simplified models provide a generic framework for analysing experimental signatures using a small number of parameters, such as masses and couplings of new fields, without reference to specific UV-complete models. Such an approach is particularly well-suited for interpreting the search for dark matter in a more model-independent way, and can be used to connect results from the LHC with dark matter searches in direct detection and from the observation of cosmic rays. Many simplified models for dark matter have been proposed in the past (see Ref. [7] and references therein). Here, we consider a simplified model with a dark matter Majorana fermion,  $\psi$ , which interacts with the SM model

---

<sup>1</sup>Limits from existing searches can sometimes be applied to new models, for example by accessing archived versions of the original analysis code and detector simulation via the RECAST [9] project, or by independent implementations of experimental searches, see, for example, Refs. [10–14].

through a new vector particle,  $Z'$ . The couplings of the mediator  $Z'$  to the dark matter  $\psi$  and to the SM are specified as

$$\mathcal{L} \supset g_{\text{DM}} \bar{\psi} \gamma_{\mu} \gamma_5 \psi Z'^{\mu} + g_q \sum_q \bar{q} \gamma_{\mu} q Z'^{\mu}, \quad (1)$$

where the sum in the second term includes the first generation SM quarks,  $q \in \{u, d\}$ . The simplified model specified in Eq. (1) has only four free parameters, two couplings and two masses:  $g_{\text{DM}}$ ,  $g_q$ ,  $M_{\psi} \equiv M_{\text{DM}}$ , and  $M_{Z'}$ . The width of the mediator,  $\Gamma_{Z'}$ , is determined by these four parameters.

Following Ref. [15] we have chosen to couple the mediator to dark matter and to the SM quarks through an axial-vector and vector current, respectively. An axial-vector coupling of the mediator to dark matter leads to spin-dependent dark matter-nucleon interactions and thus weaker bounds from direct dark matter searches. Such a coupling structure naturally arises for Majorana fermion dark matter. Having also axial-vector couplings between the mediator and the SM requires UV-completions of the simplified model in which the SM Higgs has to be charged under the  $U(1)'$  gauge group of the vector mediator. As a consequence, there is mixing between the  $Z'$  and the gauge boson of the SM, and gauge invariance requires the couplings of the  $Z'$  to be flavour universal. However, models where the mediator couples to leptons are strongly constrained by collider searches for di-lepton resonances. For vector couplings of the  $Z'$  to SM fermions, on the other hand, the SM Higgs does not carry a  $U(1)'$  charge and the charges of quarks and leptons are independent. We are thus free to set the  $Z'$  lepton coupling to zero to evade constraints from di-lepton searches, and consider a simplified model with a universal vector-coupling to SM quarks only.

The parameters of the simplified model,  $g_{\text{DM}}$ ,  $g_q$ ,  $M_{\text{DM}}$ , and  $M_{Z'}$ , are constrained by perturbative unitarity. From a partial wave analysis of the annihilation process  $\bar{\psi}\psi \rightarrow Z'Z'$  one can derive the unitarity limit [15]

$$M_{\text{DM}} \lesssim \sqrt{\frac{\pi}{2}} \frac{M_{Z'}}{g_{\text{DM}}}, \quad (2)$$

which defines the parameter space where the dark matter relic density can be reliably calculated within the simplified model. Perturbative unitarity of the scattering amplitude in processes relevant to LHC dark matter searches has been studied in Ref. [16]. It was found that perturbative unitarity is respected in the production of mediators at the LHC, unless the couplings are large,  $g_q \gtrsim \mathcal{O}(4\pi)$ . In our analysis, we will only consider couplings which are well within the perturbative regime,  $g_{\text{DM}}$ ,  $g_q \lesssim \mathcal{O}(1)$ , so that our predictions for dark matter and mediator production at the LHC are well-defined.

Dark matter has been searched for at the LHC in signatures with jets and large missing transverse momentum, see e.g. [17, 18] for recent analyses. The results [17, 18] have not been interpreted in the simplified model defined in Eq. (1), but in similar models with pure vector or axial-vector mediators and Dirac fermion dark matter. The searches probe the region where  $M_{\text{DM}} \lesssim M_{Z'}/2$  and exclude dark matter and mediator masses of up to about 500 GeV and 1.5 TeV, respectively. Similar exclusions have been obtained in simplified model re-interpretations of LHC searches as presented in, e.g., Refs. [15, 19]. Searches for dijet resonances from mediator production and decay can place further strong constraints on the dark matter simplified model as demonstrated in Refs. [20, 21].

To simulate the experimental signature for our model, we have encoded the model Lagrangian in FEYNRULES 2.3.18 [22]. Using its UFO interface [23], a BSM configuration is created for Herwig 7.0.1 [4, 5]. For each parameter point in the scan grid, events were generated in Herwig and analysed using the selected analyses implemented in Rivet 2.4.1 [8] (see section 3). Calculation of the exclusion contours was done in Python scripts, available on the CONTUR website <https://contur.hepforge.org/>.

Higher-order QCD corrections have been calculated for this class of dark matter simplified models with an  $s$ -channel vector mediator, see Refs. [24–27]. However, for the purpose of this paper where we focus on introducing the CONTUR approach rather than exploring a particular BSM theory in great detail, we will use leading-order signal cross section predictions as provided by Herwig 7. The most relevant production and decay channels for the mediator are illustrated in Fig. 1.

### 3 Measurements

To be useful in our approach, measurements must be made in as model-independent a fashion as possible. Cross sections should be measured in a kinematic region closely matching the detector acceptance — commonly called ‘fiducial cross sections’ — to avoid extrapolation into unmeasured regions, since such extrapolations must always make theoretical assumptions; usually that the SM is valid. The measurements should generally be made in terms of observable final state particles (e.g. leptons, photons) or objects constructed from such particles (e.g. hadronic jets, missing energy) rather than assumed intermediate states ( $W, Z, H, \text{top}$ ). Finally, differential measurements are most useful, as features in the shapes of distributions are a more sensitive test than simple event rates — especially when there are highly-correlated systematic experimental uncertainties, such as those on the integrated luminosity, or the jet energy scale.

One feature noted in several cases is that missing transverse energy ( $E_T^{\text{miss}}$ ) is explicitly assumed to be the same as neutrino transverse energy. In BSM physics, missing energy can also arise from other sources (for example, dark matter production) and so it is important that the result is treated in such a way that this sensitivity is correctly estimated. The measurements are typically corrected back to total  $E_T^{\text{miss}}$ , or to the assumed neutrino  $p_T$ , in the experimental analysis, using a simulated SM event sample which has been shown to describe the data well. This involves an extrapolation into the forward region where transverse energy is unmeasured; however, unless a BSM particle enters this region, the error made is negligible. This means that as long as (in the Rivet analysis) a fiducial acceptance cut is made on BSM particles counting toward  $E_T^{\text{miss}}$  (to ensure that large contributions to  $E_T^{\text{miss}}$  from invisible particles outside the detector acceptance are excluded) such measurements can be used.<sup>2</sup>

Another feature of the measurements is that most of them, explicitly or implicitly, insist in their fiducial cross-section definition that leptons and photons be ‘directly’ produced, that is, prior to hadronisation and coming from the primary vertex of the collision. Such a selection is enforced in the experiments by a mixture of isolation and vertex requirements, but is not universally enforced in all Rivet routines. Generally this is a small effect, but care needs to be taken that the sensitivity is not overestimated, especially for BSM models which enhance bottom or charm production, when semi-leptonic decays may play a role. This feature will be addressed in future releases of Rivet.

The measurements we consider fall into five loose and independent classes.

1. Jets: event topologies with any number of jets but no missing energy, leptons, or photons. In this category there are important measurements from both ATLAS and CMS, many of which have existing Rivet analyses. We make use of the highest integrated-luminosity inclusive [28,29], dijet [30,31] and three-jet [32] measurements made in 7 TeV collisions, as well as the jet mass measurement from CMS [33]. Unfortunately results from 8 TeV collisions are rarer, and the only one we can use currently is the four-jet measurement from ATLAS [34].
2. Electroweak: events with leptons, with or without missing energy or photons. The high-statistics  $W$ +jet and  $Z$ +jet measurements from ATLAS [35,36] and CMS [37,38], are used. We also use the ATLAS  $ZZ$  and  $W/Z + \gamma$  analyses [39,40], the former of which includes  $E_T^{\text{miss}}$ , via the  $Z \rightarrow \nu\bar{\nu}$  measurement.
3. Missing energy, possibly with jets but no leptons or photons. This channel could in principle provide powerful constraints, and has been used in searches (see for example [41]). Unfortunately however, there are currently no fully-corrected particle-level distributions available in this category.
4. Isolated photons, with or without missing energy, but no leptons. Here we make use of the inclusive [42], diphoton [43] and photon-plus-jet [44] measurements, where available. We also made a new Rivet routine for the CMS photon-plus jet measurement [45].
5. Signatures specifically based on top quark or Higgs candidates. Most such measurements to date have been made at the ‘parton’ level (that is, corrected using SM MC back to the top

---

<sup>2</sup>Of greater consequence, but easier to fix, is the fact that several Rivet methods explicitly calculated  $E_T^{\text{miss}}$  from neutrinos found in the simulated event record, rather than as the negative of the visible particles in the event. These routines were modified as a part of this work, and are fixed in future Rivet releases.

or Higgs before decay), and many of them are extrapolated to  $4\pi$  phase space. Both steps increase the model dependence and make them unsuitable for the CONTUR approach. Recently, however, fiducial, differential, particle-level measurements have begun to appear [46,47]. These are potentially very powerful in excluding some models, but will in principle overlap with the previous categories depending on decay mode. We leave the inclusion of such measurements for future work.

The choice of which measurements are actually included at this stage is driven mainly by the availability of particle-level differential fiducial cross sections implemented in Rivet. The current selection is summarised in Table 1.

CONTUR Category	Rivet/ Inspire ID	Rivet description
ATLAS 7 Jets	ATLAS_2014_I1325553 [28]	Measurement of the inclusive jet cross-section
	ATLAS_2014_I1268975 [30]	High-mass dijet cross section
	ATLAS_2014_I1326641 [32]	3-jet cross section
	ATLAS_2014_I1307243 [31]	Measurements of jet vetoes and azimuthal decorrelations in dijet events
CMS 7 Jets	CMS_2014_I1298810 [29]	Ratios of jet pT spectra, which relate to the ratios of inclusive, differential jet cross sections
ATLAS 8 Jets	ATLAS_2015_I1394679 [34]	Multijets at 8 TeV
ATLAS 7 Z Jets	ATLAS_2013_I1230812 [35]	Z + jets
CMS 7 Z Jets	CMS_2015_I1310737 [38]	Jet multiplicity and differential cross-sections of Z+jets events
CMS 7 W Jets	CMS_2014_I1303894 [37]	Differential cross-section of W bosons + jets
ATLAS 7 W jets	ATLAS_2014_I1319490 [36]	W + jets
ATLAS 7 Photon Jet	ATLAS_2013_I1263495 [42]	Inclusive isolated prompt photon analysis with 2011 LHC data
	ATLAS_2012_I1093738 [44]	Isolated prompt photon + jet cross-section
CMS 7 Photon Jet	CMS_2014_I1266056 [45]	Photon + jets triple differential cross-section
ATLAS 7 Diphoton	ATLAS_2012_I1199269 [43]	Inclusive diphoton +X events
ATLAS 7 ZZ	ATLAS_2012_I1203852 [39]	Measurement of the ZZ(*) production cross-section
ATLAS W/Z gamma	ATLAS_2013_I1217863 [40]	W/Z gamma production

Table 1: Table of all Rivet routines currently included in the limit-setting scan. With the one indicated exception, they are all based on 7 TeV data.

## 4 Method

### 4.1 Strategy

The approach taken is to consider simplified BSM models in the light of existing measurements which have *already been shown to agree* with SM expectations. Thus this is inherently an exercise in limit-setting rather than discovery. The assumption is that a generic, measurement-based approach such as this will not be competitive in terms of sensitivity, or speed of discovery, with a dedicated search for a specific BSM final-state signature. However, it will have the advantage of breadth of coverage, and will make a valuable contribution to physics at the energy frontier whether or not new signatures are discovered at the LHC. In the case of a new discovery, many models will be put forward to explain the data, as has for example already been seen [48] after the 750 GeV diphoton anomaly reported by ATLAS and CMS at the end of 2015 and start of 2016 [49,50]. Checking these models for consistency with existing measurements will be vital for unravelling whatever the data might be telling us. As will be shown in subsequent sections, models designed to explain one signature may have somewhat unexpected consequences in different final states, some of which have already been precisely measured. If it should turn out that no BSM signatures are in the end confirmed at the LHC, CONTUR offers

potentially the broadest and most generic constraints on new physics, and motivates the most precise possible model-independent measurements over a wide range of final states, giving the best chance of an indirect pointer to the eventual scale of new physics. Given this strategy, possible treatments of the data present themselves. The most complete is to take precision SM calculations to define the background, with their associated uncertainties, and superimpose the putative signal, and check for consistency with the data within uncertainties. However, for striking signals such as those considered here, and for data which have already been shown to exhibit no such striking features and indeed to agree with SM calculations, it is reasonable and much more efficient to make the assumption for such measurements that the data are the SM, and to take the uncertainties on the data as defining the room that is left for BSM signatures. Neither approach treats interference effects properly – this would require a full final-state calculation including all SM and BSM diagrams, which are in general not available. In this initial study, we follow the second approach, although future plans include incorporating SM predictions and their uncertainties directly.

## 4.2 Dynamical data selection

Starting with the measurements discussed in Section 3 we define a procedure to combine exclusion limits from different measured distributions. The data used for comparison in Rivet come in the form of histograms, which do not carry information about the correlations between uncertainties — even when in several cases detailed information is made available in the experimental papers. There are highly correlated uncertainties in several measurements, for example on the integrated luminosity, or the energy scale of jet measurements. In some cases these are dominant. Including correlations would be a highly complex process, since as well as correlations within a single data-set, there are also common systematic uncertainties between different results, which are generally not provided by the experiments. There are also overlaps between event samples used in many different measurements, which lead to non-trivial correlations in the statistical uncertainties. To attempt to avoid spuriously high exclusion rates due to multiply-counting what might be the same exclusion against several datasets, we take the following approach:

1. Divide the measurements into groups that have no overlap in the event samples used, and hence no statistical correlation between them. These measurements are grouped by, crudely, different final states, different experiments, and different beam energies (see Table 1).
2. Scan within each group for the most significant deviation between BSM+SM and SM. This is done distribution-by-distribution and bin-by-bin within distributions. Use only the most significant deviation, and disregard the rest. Although the selection of the most significant deviation sounds intuitively suspect, in our case it is a conservative approach, since we make the assumption that the data are equal to the SM, and discarding the less-significant bins simply reduces sensitivity. The use of a single bin from each measured distribution removes the dominant effect of highly correlated systematic uncertainties within a single measurement. Where several of statistically-independent distributions exists *within* a group, their likelihoods may be combined to give a single likelihood ratio from the group, on the assumption that the systematic correlations between distributions are reduced compared to those within a single distribution.
3. Combine the likelihood ratios of the different groups to give a single exclusion limit.

## 4.3 Statistical Method

The question we wish to ask of any given BSM proposal is ‘*at what significance do existing measurements, which agree with the SM, already exclude this?*’. For all the measurements considered, comparisons to SM calculations have shown consistency between them and the data. Thus as a starting point, we take the data as our “null signal”, and we superpose onto them the contribution from the BSM scenario under consideration. The uncertainties on the data will define the allowed space for these extra BSM contributions.

Taking each bin of each distribution considered as a separate statistic to be tested, a likelihood function for each bin can be constructed as follows,

$$L(\mu, b, \sigma_b, s) = \frac{(\mu s + b)^n}{n!} \exp(-(\mu s + b)) \times \frac{1}{\sqrt{2\pi}\sigma_b} \exp\left(-\frac{(m-b)^2}{2\sigma_b^2}\right) \times \frac{(\tau s)^k}{k!} \exp(-\tau s), \quad (3)$$

where the three factors are:

- A Poisson event count, noting that the measurements considered are differential cross section measurements, hence the counts are multiplied by a factor of the integrated luminosity taken from the experimental paper behind each analysis, to convert to an event count in each bin (and subsequently the additional events that the new physics would have added to the measurement made). This statistic in each tested bin then is comprised of:
  - $s$ , the parameter defining the BSM signal event count.
  - $b$ , the parameter defining the background event count.
  - $n$ , the observed event count.
  - $\mu$ , the signal strength parameter modulating the strength of the signal hypothesis tested, thus  $\mu = 0$  corresponds to the background-only hypothesis and  $\mu = 1$  the full signal strength hypothesis;
- A convolution with a Gaussian defining the distribution of the background count, where the following additional components are identified:
  - $m$ , the background count. The expectation value of this count, which is used to construct the test, is taken as the central value of the measured data point.
  - $\sigma_b$ , the uncertainty in the background event count taken, from the data, as  $1 \sigma$  error on a Gaussian (uncertainties taken as the combination of statistical and systematics uncertainties in quadrature. Typically the systematic uncertainty dominates).
- An additional Poisson term describing the Monte Carlo error on the simulated BSM signal count with  $k$  being the actual number of generated BSM events. The expectation value of  $k$  is related to  $s$  by a factor  $\tau$ , which is the ratio of the generated MC luminosity to the experimental luminosity.

This likelihood is then used to construct a test statistic based on the profile likelihood ratio, following the arguments laid out in Ref. [51]. In particular, the  $\tilde{q}_\mu$  test statistic is constructed. This enables the setting of a one-sided upper limit on the confidence in the strength parameter hypothesis,  $\mu$ , desirable since in the situation that the observed strength parameter exceeds the tested hypothesis, agreement with the hypothesis should not diminish. In addition this construction places a lower limit on the strength parameter, where any observed fluctuations below the background-only hypothesis are said to agree with the background-only hypothesis<sup>3</sup>. The required information then is the sampling distribution of this test statistic. This can either be evaluated either using the so called Asimov data set to build an approximate distribution of the considered test statistic, or explicitly using multiple Monte Carlo ‘toy model’ tests<sup>4</sup>.

The information needed to build the approximate sampling distributions is contained in the covariance matrix composed of the second derivatives with respect to the parameters ( $\mu, b$  and  $s$ ), of

---

<sup>3</sup>At present, the latter point will be unimportant, as the manner in which samples are generated and tested will only increase the event rates with respect to the background-only hypothesis.

<sup>4</sup>For the cases considered here the results were found to be equivalent, implying that the tested parameter space values fall into the asymptotic, or large sample, limit, and so the Asimov approach is used.

the log of the likelihood given in equation 3. They are as follows:

$$\begin{aligned}
\mu\mu : & \quad \frac{\partial^2 \ln L}{\partial \mu^2} = \frac{-ns^2}{(\mu s + b)^2} \\
bb : & \quad \frac{\partial^2 \ln L}{\partial b^2} = \frac{-n}{(\mu s + b)^2} - \frac{1}{\sigma_b^2} \\
ss : & \quad \frac{\partial^2 \ln L}{\partial s^2} = \frac{-n\mu^2}{(\mu s + b)^2} - \frac{k}{s^2} \\
\mu s = s\mu : & \quad \frac{\partial^2 \ln L}{\partial \mu \partial s} = \frac{nb}{(\mu s + b)^2} - 1 \\
\mu b = b\mu : & \quad \frac{\partial^2 \ln L}{\partial \mu \partial b} = \frac{-ns}{(\mu s + b)^2} \\
bs = sb : & \quad \frac{\partial^2 \ln L}{\partial s \partial b} = \frac{-n\mu}{(\mu s + b)^2}.
\end{aligned}$$

Which are arranged in the inverse covariance matrix as follows.

$$V^{-1} = -E \begin{bmatrix} \mu\mu & \mu s & \mu b \\ s\mu & ss & sb \\ b\mu & bs & bb \end{bmatrix} \quad (4)$$

The variance of  $\mu$  is extracted from the inverse of the matrix given in eq.4 as;

$$\sigma_\mu^2 = V_{\mu,\mu} \quad (5)$$

In order to evaluate this, the counting parameters ( $n, m$  and  $k$ ) are evaluated at their Asimov values, following arguments detailed in Ref. [51]. These are taken as follows,

- $n_A = E[n] = \mu' s + b$ . The total count under the assumed signal strength,  $\mu'$ , which for the purposes of this argument is equal to 1
- $m_A = E[m] = b$ . The background count is defined as following a Gaussian distribution with a mean of  $b$ .
- $k_A = E[k] = \tau s$ . The signal count is defined following a Poisson distribution with a mean of  $\tau s$

Using this data set the variance of the strength parameter,  $\mu$ , under the assumption of a hypothesised value,  $\mu'$ , can be found. This is then taken to define the distribution of the  $\tilde{q}_\mu$  statistic, and consequently the size of test corresponding to the observed value of the count. The size of the test can be quoted as a  $p$ -value, or equivalently the confidence level which is the inverse of the size of the test. As is convention in the particle physics community, the final measure of statistical agreement is presented in terms of what is known as the  $CL_s$  method [54, 55]. Then, for a given distribution,  $CL_s$  can be evaluated separately for each bin, where the bin with the largest  $CL_s$  value (and correspondingly smallest  $p_{s+b}$  value) is taken to represent the sensitivity measure used to evaluate each distribution, a process outlined in section 4.2.

Armed then with a list of selected sensitive distributions with minimal correlations, a total combined  $CL_s$  across all considered channels can then be constructed from the product of the likelihoods. This leaves the core of the methodology presented here unchanged, the effect is simply extending the covariances matrix. The overall result gives a probability, for each tested parameter set, that the observed counts  $n_i$ , across all the measurement bins considered, are compatible with the full signal strength hypothesis.

Finally it is noted that this methodology has been designed to simply profile BSM contributions against data taken. This can be extended to incorporate a separate background simulation or include correlation between bins where available.

## 4.4 Limitations

We note that our method is best adapted to identifying kinematic features (mass peaks, kinematic edges) and will be less sensitive to smooth deviations in normalisation. In particular, since we take the data to be identically equal to the SM expectation, we will be insensitive to a signal which might in principle arise as the cumulative effect of a number of statistically insignificant deviations across a range of experimental measurements. No such effects are apparent when studying the model considered here, but quantifying this statement is beyond the scope of the current work, and requires an extensive evaluation of the theoretical uncertainties on the SM predictions for each channel. This is an extension of the method planned for future work. Additionally, in low statistics regions, outlying events in the tails of the data will not lead to a weakening of the limit, as would be the case in a search. However, measurements unfolded to the particle-level are typically performed in bins with a requirement of minimum number of events in any given bin, reducing the impact of this effect. Our limits focus on the impact of high precision measurements on the BSM model, in which systematic uncertainties typically dominate. For these reasons, the limits derived are described as expected limits, although in regions where the confidence level is high, they do represent a real exclusion.

## 5 Comparison to Data

To investigate the exclusion power of the SM measurements discussed in Section 3 we scan a range in plausible mediator masses ( $M_{Z'}$ ) and dark matter masses ( $M_{\text{DM}}$ ) within the model described in Section 2, for three choices of the coupling of the mediator to the SM ( $g_q$ ). These coupling choices correspond to (i) an ‘optimistic’ scenario  $g_q = 0.5, g_{\text{DM}} = 1$ : strong signals, close to the edge of exclusion already, (ii) a ‘challenging’ scenario  $g_q = 0.25, g_{\text{DM}} = 1$ : low couplings, hard to exclude, and (iii) an ‘intermediate’ scenario  $g_q = 0.375, g_{\text{DM}} = 1$ , between the two. We also consider (iv) a scenario where the coupling of dark matter to the mediator is suppressed,  $g_q = 0.375, g_{\text{DM}} = 0.25$ . For all these scenarios, the calculated width of the mediator is less than 10% of  $M_{Z'}$ , as shown in Table 2.

$g_q$	$g_{\text{DM}}$	$M_{Z'}$ [GeV]	$M_{\text{DM}}$ [GeV]	$\Gamma_{Z'}/M_{Z'}$
0.25	1	3000	100	0.0626
0.375	1	3000	100	0.0751
0.5	1	3000	100	0.0925
0.375	0.25	3000	100	0.0257

Table 2: Table of maximal  $\Gamma_{Z'}/M_{Z'}$  occurring over the mass ranges for the four heatmaps shown in Figure 6

Figure 2 shows a comparison between the model expectations in the ‘intermediate’ scenario and the most sensitive distributions from the ATLAS jet measurements. The measured dijet mass distribution is smoothly falling to higher masses, and the presence of a mediator decaying to quarks (see Fig.1a and 1b) would superimpose a peak, not seen in the data, thus leading to an exclusion. The results are shown for fixed  $M_{\text{DM}} = 600$  GeV and a range of mediator masses  $500 < M_{Z'} < 2000$  GeV. The sensitivity is at maximum in the middle of this range.

Figure 3 shows a similar comparison for a comparable measurement from CMS. This time the sensitivity is in the jet  $p_{\text{T}}$  distribution, but the pattern is similar, with a maximal sensitivity for mediator masses around 1 TeV. These measurements typify the sensitivities obtained from the ‘Jets’ measurements discussed in Section 3. It is notable that 7 TeV measurements form the bedrock of the exclusions. This is due to the lack of availability of precision 8 TeV and 13 TeV measurements in Rivet. Such measurements are likely to be available soon and can be expected to significantly improve the exclusion power of these final states.

Moving on to the ‘electroweak’ final states discussed in Section 3, Figure 4 illustrates the sensitivity of vector-boson-plus-jet ( $V+\text{jet}$ ) measurements to this model, in this case the dijet mass differential

cross section in  $W+$ -jet events. Strictly speaking, the measurement is made for events with a single charged lepton,  $E_T^{\text{miss}}$ , and jets, interpreted as  $W$ +jets in the SM. In the BSM model considered here,  $E_T^{\text{miss}}$  could in principle also arise from the dark matter candidate. However, inspections shows that the sensitivity, which is at mediator masses below around a TeV or so, arises from genuine  $W$  bosons produced in association with the mediator — see Fig. 1c — which is not a signature typically considered in constraints on this class of model. The sensitivity is obviously highly dependent upon the bin width chosen in the SM measurement, which is driven mainly by the dijet mass resolution, although at high masses also by the number of events in the data.

Also in the ‘electroweak’ category are the diboson measurements. Here the most sensitive is the ATLAS  $ZZ$  measurement, in particular the 7 TeV result, which includes a fiducial cross section measurement of  $pp \rightarrow l^+l^- + E_T^{\text{miss}}$ , interpreted in the paper as  $pp \rightarrow ZZ \rightarrow l^+l^- \nu\bar{\nu}$ , but performed in a sufficiently model-independent fashion that it has the same sensitivity to the  $l^+l^- +$  dark matter channel. This is illustrated in Fig. 5. The production diagrams are the same as the  $V$ -jets case, Fig.1c, but in this case the mediator decays to dark matter rather than back to quarks. In the absence of any particle-level measurements in the ‘missing energy plus jets’ category of Section 3, this measurement has the best sensitivity to dark matter production for this model. Obviously, measurements at 8 TeV and 13 TeV of this final state, and indeed of jets+ $E_T^{\text{miss}}$ , can be expected to improve the sensitivity significantly.

Finally, although they were scanned in the limit-setting process, the currently available isolated photon measurements do not contribute significantly to the exclusion limits for this model.

## 6 Limits

The sensitivities derived from multiple distributions such as those discussed in the previous section are combined into ‘heatmaps’ which delineate exclusion regions and contours in the parameter space of  $M_{\text{DM}}$  and  $M_{Z'}$ . These are shown in Fig. 6 for the four  $g_q$  and  $g_{\text{DM}}$  combinations considered.

As expected, the exclusion is much weaker in the ‘challenging’ case and quite strong in the ‘optimistic’ scenario. For the first three scenarios, at  $M_{Z'} > 2M_{\text{DM}}$  the decay of the mediator to dark matter dominates over the decay to jets. This leads to the diagonal structure across the plots, with the sensitivity above the diagonal, in the left portion of the map, coming mainly from the jet measurements. In the fourth scenario, even when the decay to DM is kinematically allowed, the jet signatures continue to contribute, and so the diagonal structure is less visible.

At low values of  $M_{Z'}$  the sensitivity comes mainly from the  $V$ +jets signatures. In the challenging scenario, a dip in sensitivity around  $M_{Z'} \approx 700$  GeV is visible, where the sensitivity from inclusive jets and  $V$ +jets do not quite overlap. In the optimistic scenario, they overlap, and the whole upper left region of the map is excluded. In addition, the cross section  $\times$  branching ratio for quarks  $\rightarrow Z' \rightarrow$  quarks remains large enough that the diagonal cutoff in sensitivity of the jet channels at  $M_{Z'} \approx 2M_{\text{DM}}$  is blurred.

To the bottom right region of the diagonal the decay of the mediator to dark matter is kinematically allowed, and for  $g_{\text{DM}} = 1$  it will dominate over the decay to quarks. Hence the sensitivity in the inclusive jet (and  $V$ +jet) signatures drops in all scenarios except the fourth. This is the region where a measurement of  $E_T^{\text{miss}} +$  jets would be useful (and indeed it is where the searches performed using such signatures contribute, see, for example, [15, 19]). Current sensitivity in the intermediate and challenging scenarios comes from the  $l^+l^- + E_T^{\text{miss}}$  measurement, and dies away at  $M_{Z'} \approx 750$  GeV. In the fourth scenario, the decays to dark matter are relatively suppressed and so the  $l^+l^- + E_T^{\text{miss}}$  signature makes little contribution. However, as already discussed, the exclusion from the jet measurements remains strong.

The 90% contours derived from the heatmaps of Fig. 6 are shown in Fig. 7. Note that as expected, the sensitivity from the 7 TeV dijet measurements used here is qualitatively similar, but inferior, to the exclusions obtained combining the searches in 8 TeV and 13 TeV jet data — see, for example, [21]. This should change once measurements are available from these later running periods (indeed, the CMS measurement is already made [56], but is not yet available in Rivet or HepData). The other channels extend the sensitivity, and this will also improve as more measurements are incorporated.

As mentioned in section 2, the parameters of the simplified model are constrained by perturbative unitarity. In the region  $M_{\text{DM}} \gtrsim \sqrt{\pi/2} M_{Z'}/g_{\text{DM}}$ , indicated by the blue shaded area in Fig. 7, the

dark matter relic density cannot be calculated reliably [15]. Since we only consider couplings  $g_{\text{DM}}$  and  $g_q$  well within the perturbative regime, perturbative unitarity is respected in the production of mediators at the LHC and does not provide any further restrictions on the parameter space of our model [16]. The physics of dark matter is, of course, constrained by astrophysical and cosmological observations, including in particular the dark matter relic density, and direct and indirect searches for dark matter, see, for example, Refs. [15, 19, 57] for combined analyses of collider and astrophysical constraints of simplified dark matter models with vector mediators. However, all those constraints are based on additional assumptions on the thermal history of the Universe and astrophysical properties of dark matter, and they do not affect BSM searches at the LHC. Since we have adopted the simplified dark matter model to illustrate the power of the CONTUR approach for BSM searches at the LHC in general, rather than providing a detailed cosmological and astrophysical analysis of dark matter, we do not show the corresponding constraints in Fig. 7.

## 7 Conclusions

Using a simplified model for weakly-interacting dark matter coupled to the Standard Model via a heavy mediator vector boson, we have developed and demonstrated a method to efficiently scan existing particle-level measurements from the LHC, implemented in Rivet, to derive expected limits on new physics. The CONTUR method uses measurements which have already been shown to be in good agreement with the SM, and thus is purely aimed at limiting the possibilities for models of new physics and hopefully narrowing the focus of experimental and theoretical effort on to the best models. It is thus complementary to direct and dedicated searches. The expected exclusion limits obtained are competitive with limits from searches to date which have reported null results. One notable feature is the simultaneous coverage of a wide variety of final states. This leads to enhanced stability of the sensitivity as a function of model parameters, and also can uncover sensitivity in channels which might not otherwise be considered. For example, in our case unexpected sensitivity is seen in  $V$ +jets measurements, as well as the more commonly used dijet and  $E_T^{\text{miss}}$  channels. Future plans include better treatment of correlated uncertainties and the incorporation of SM predictions and uncertainties directly into Contur, rather than relying on previous comparisons. The method is highly scaleable to new measurements as they are produced, and to new simplified models as they are developed.

## Acknowledgments

This work started at the ‘Interdisciplinary Workshop on Models, simulations and data at LHC’ in Edinburgh, and continued in the 2015 Les Houches meeting on TeV-scale physics and two MCnet schools in Göttingen. The authors thank the organisers, especially Michela Massimi, Fawzi Boudjema and Steffen Schumann. They also thank Josh McFayden for useful discussions, and STFC for financial support. This work was supported in part by the European Union as part of the FP7 Marie Curie Initial Training Network MCnetITN (PITN-GA-2012-315877). MK is supported by the German Research Foundation DFG through the research unit 2239 “New physics at the LHC”.

## References

- [1] ATLAS COLLABORATION collaboration, G. Aad et al., *Observation of a new particle in the search for the Standard Model Higgs boson with the ATLAS detector at the LHC*, *Phys.Lett.* **B716** (2012) 1–29, [1207.7214].
- [2] CMS COLLABORATION collaboration, S. Chatrchyan et al., *Observation of a new boson at a mass of 125 GeV with the CMS experiment at the LHC*, *Phys.Lett.* **B716** (2012) 30–61, [1207.7235].
- [3] A. Buckley et al., *General-purpose event generators for LHC physics*, *Phys. Rept.* **504** (2011) 145–233, [1101.2599].

- [4] J. Bellm et al., *Herwig 7.0/Herwig++ 3.0 release note*, *Eur. Phys. J.* **C76** (2016) 196, [1512.01178].
- [5] M. Bahr et al., *Herwig++ Physics and Manual*, *Eur. Phys. J.* **C58** (2008) 639–707, [0803.0883].
- [6] LHC NEW PHYSICS WORKING GROUP collaboration, D. Alves, *Simplified Models for LHC New Physics Searches*, *J. Phys.* **G39** (2012) 105005, [1105.2838].
- [7] D. Abercrombie et al., *Dark Matter Benchmark Models for Early LHC Run-2 Searches: Report of the ATLAS/CMS Dark Matter Forum*, 2015.
- [8] A. Buckley, J. Butterworth, L. Lonnblad, D. Grellscheid, H. Hoeth et al., *Rivet user manual*, *Comput.Phys.Commun.* **184** (2013) 2803–2819, [1003.0694].
- [9] K. Cranmer and I. Yavin, *RECAST: Extending the Impact of Existing Analyses*, *JHEP* **04** (2011) 038, [1010.2506].
- [10] E. Conte, B. Fuks and G. Serret, *MadAnalysis 5, A User-Friendly Framework for Collider Phenomenology*, *Comput. Phys. Commun.* **184** (2013) 222–256, [1206.1599].
- [11] M. Drees, H. Dreiner, D. Schmeier, J. Tattersall and J. S. Kim, *CheckMATE: Confronting your Favourite New Physics Model with LHC Data*, *Comput. Phys. Commun.* **187** (2015) 227–265, [1312.2591].
- [12] S. Kraml, S. Kulkarni, U. Laa, A. Lessa, W. Magerl, D. Proschofsky-Spindler et al., *SModelS: a tool for interpreting simplified-model results from the LHC and its application to supersymmetry*, *Eur. Phys. J.* **C74** (2014) 2868, [1312.4175].
- [13] M. Papucci, K. Sakurai, A. Weiler and L. Zeune, *Fastlim: a fast LHC limit calculator*, *Eur. Phys. J.* **C74** (2014) 3163, [1402.0492].
- [14] D. Barducci, A. Belyaev, M. Buchkremer, G. Cacciapaglia, A. Deandrea, S. De Curtis et al., *Framework for Model Independent Analyses of Multiple Extra Quark Scenarios*, *JHEP* **12** (2014) 080, [1405.0737].
- [15] F. Kahlhoefer, K. Schmidt-Hoberg, T. Schwetz and S. Vogl, *Implications of unitarity and gauge invariance for simplified dark matter models*, *JHEP* **02** (2016) 016, [1510.02110].
- [16] C. Englert, M. McCullough and M. Spannowsky, *S-Channel Dark Matter Simplified Models and Unitarity*, 1604.07975.
- [17] ATLAS collaboration, M. Aaboud et al., *Search for new phenomena in final states with an energetic jet and large missing transverse momentum in pp collisions at  $\sqrt{s} = 13$  TeV using the ATLAS detector*, 1604.07773.
- [18] CMS collaboration, C. Collaboration, *Search for dark matter production in association with jets, or hadronically decaying W or Z boson at  $\sqrt{s} = 13$  TeV*, .
- [19] J. Heisig, M. Krämer, M. Pellen and C. Wiebusch, *Constraints on Majorana Dark Matter from the LHC and IceCube*, *Phys. Rev.* **D93** (2016) 055029, [1509.07867].
- [20] M. Chala, F. Kahlhoefer, M. McCullough, G. Nardini and K. Schmidt-Hoberg, *Constraining Dark Sectors with Monojets and Dijets*, *JHEP* **07** (2015) 089, [1503.05916].
- [21] M. Fairbairn, J. Heal, F. Kahlhoefer and P. Tunney, *Constraints on Z' models from LHC dijet searches*, 1605.07940.
- [22] A. Alloul, N. D. Christensen, C. Degrande, C. Duhr and B. Fuks, *FeynRules 2.0 - A complete toolbox for tree-level phenomenology*, *Comput. Phys. Commun.* **185** (2014) 2250–2300, [1310.1921].

- [23] C. Degrande, C. Duhr, B. Fuks, D. Grellscheid, O. Mattelaer and T. Reiter, *UFO - The Universal FeynRules Output*, *Comput. Phys. Commun.* **183** (2012) 1201–1214, [1108.2040].
- [24] P. J. Fox and C. Williams, *Next-to-Leading Order Predictions for Dark Matter Production at Hadron Colliders*, *Phys. Rev.* **D87** (2013) 054030, [1211.6390].
- [25] U. Haisch, F. Kahlhoefer and E. Re, *QCD effects in mono-jet searches for dark matter*, *JHEP* **12** (2013) 007, [1310.4491].
- [26] M. Backovi, M. Krämer, F. Maltoni, A. Martini, K. Mawatari and M. Pellen, *Higher-order QCD predictions for dark matter production at the LHC in simplified models with s-channel mediators*, *Eur. Phys. J.* **C75** (2015) 482, [1508.05327].
- [27] M. Neubert, J. Wang and C. Zhang, *Higher-Order QCD Predictions for Dark Matter Production in Mono-Z Searches at the LHC*, *JHEP* **02** (2016) 082, [1509.05785].
- [28] ATLAS collaboration, G. Aad et al., *Measurement of the inclusive jet cross-section in proton-proton collisions at  $\sqrt{s} = 7$  TeV using 4.5 fb<sup>1</sup> of data with the ATLAS detector*, *JHEP* **02** (2015) 153, [1410.8857].
- [29] CMS collaboration, S. Chatrchyan et al., *Measurement of the ratio of inclusive jet cross sections using the anti- $k_T$  algorithm with radius parameters  $R=0.5$  and  $0.7$  in pp collisions at  $\sqrt{s} = 7$  TeV*, *Phys. Rev.* **D90** (2014) 072006, [1406.0324].
- [30] ATLAS collaboration, G. Aad et al., *Measurement of dijet cross sections in pp collisions at 7 TeV centre-of-mass energy using the ATLAS detector*, *JHEP* **05** (2014) 059, [1312.3524].
- [31] ATLAS collaboration, G. Aad et al., *Measurements of jet vetoes and azimuthal decorrelations in dijet events produced in pp collisions at  $\sqrt{s} = 7$  TeV using the ATLAS detector*, *Eur. Phys. J.* **C74** (2014) 3117, [1407.5756].
- [32] ATLAS collaboration, G. Aad et al., *Measurement of three-jet production cross-sections in pp collisions at 7 TeV centre-of-mass energy using the ATLAS detector*, *Eur. Phys. J.* **C75** (2015) 228, [1411.1855].
- [33] CMS collaboration, S. Chatrchyan et al., *Studies of jet mass in dijet and W/Z + jet events*, *JHEP* **05** (2013) 090, [1303.4811].
- [34] ATLAS collaboration, G. Aad et al., *Measurement of four-jet differential cross sections in  $\sqrt{s} = 8$  TeV proton-proton collisions using the ATLAS detector*, *JHEP* **12** (2015) 105, [1509.07335].
- [35] ATLAS collaboration, G. Aad et al., *Measurements of the W production cross sections in association with jets with the ATLAS detector*, *Eur. Phys. J.* **C75** (2015) 82, [1409.8639].
- [36] ATLAS collaboration, G. Aad et al., *Measurement of the production cross section of jets in association with a Z boson in pp collisions at  $\sqrt{s} = 7$  TeV with the ATLAS detector*, *JHEP* **07** (2013) 032, [1304.7098].
- [37] CMS collaboration, V. Khachatryan et al., *Differential cross section measurements for the production of a W boson in association with jets in proton-proton collisions at  $\sqrt{s} = 7$  TeV*, *Phys. Lett.* **B741** (2015) 12–37, [1406.7533].
- [38] CMS collaboration, V. Khachatryan et al., *Measurements of jet multiplicity and differential production cross sections of Z+ jets events in proton-proton collisions at  $\sqrt{s} = 7$  TeV*, *Phys. Rev.* **D91** (2015) 052008, [1408.3104].
- [39] ATLAS collaboration, G. Aad et al., *Measurement of ZZ production in pp collisions at  $\sqrt{s} = 7$  TeV and limits on anomalous ZZZ and ZZ $\gamma$  couplings with the ATLAS detector*, *JHEP* **03** (2013) 128, [1211.6096].

- [40] ATLAS collaboration, G. Aad et al., *Measurements of  $W\gamma$  and  $Z\gamma$  production in  $pp$  collisions at  $\sqrt{s}=7\text{TeV}$  with the ATLAS detector at the LHC*, *Phys. Rev.* **D87** (2013) 112003, [1302.1283].
- [41] ATLAS collaboration, G. Aad et al., *Search for squarks and gluinos with the ATLAS detector in final states with jets and missing transverse momentum using  $4.7\text{fb}^{-1}$  of  $\sqrt{s} = 7\text{TeV}$  proton-proton collision data*, *Phys. Rev.* **D87** (2013) 012008, [1208.0949].
- [42] ATLAS collaboration, G. Aad et al., *Measurement of the inclusive isolated prompt photons cross section in  $pp$  collisions at  $\sqrt{s} = 7\text{TeV}$  with the ATLAS detector using  $4.6\text{fb}^{-1}$* , *Phys. Rev.* **D89** (2014) 052004, [1311.1440].
- [43] ATLAS collaboration, G. Aad et al., *Measurement of isolated-photon pair production in  $pp$  collisions at  $\sqrt{s} = 7\text{TeV}$  with the ATLAS detector*, *JHEP* **01** (2013) 086, [1211.1913].
- [44] ATLAS collaboration, G. Aad et al., *Measurement of the production cross section of an isolated photon associated with jets in proton-proton collisions at  $\sqrt{s} = 7\text{TeV}$  with the ATLAS detector*, *Phys. Rev.* **D85** (2012) 092014, [1203.3161].
- [45] CMS collaboration, S. Chatrchyan et al., *Measurement of the triple-differential cross section for photon+jets production in proton-proton collisions at  $\sqrt{s}=7\text{TeV}$* , *JHEP* **06** (2014) 009, [1311.6141].
- [46] ATLAS collaboration, G. Aad et al., *Measurement of the differential cross-section of highly boosted top quarks as a function of their transverse momentum in  $\sqrt{s} = 8\text{TeV}$  proton-proton collisions using the ATLAS detector*, *Phys. Rev.* **D93** (2016) 032009, [1510.03818].
- [47] CMS collaboration, V. Khachatryan et al., *Measurement of the integrated and differential  $t$ -bar production cross sections for high-pt top quarks in  $pp$  collisions at  $\sqrt{s} = 8\text{TeV}$* , 1605.00116.
- [48] R. Garisto, *Editorial: Theorists react to the cern 750 gev diphoton data*, *Phys. Rev. Lett.* **116** (Apr, 2016) 150001.
- [49] *Search for resonances in diphoton events with the ATLAS detector at  $\sqrt{s} = 13\text{TeV}$* , Tech. Rep. ATLAS-CONF-2016-018, CERN, Geneva, Mar, 2016.
- [50] CMS COLLABORATION collaboration, *Search for new physics in high mass diphoton events in  $3.3\text{fb}^{-1}$  of proton-proton collisions at  $\sqrt{s} = 13\text{TeV}$  and combined interpretation of searches at 8 TeV and 13 TeV*, Tech. Rep. CMS-PAS-EXO-16-018, CERN, Geneva, 2016.
- [51] G. Cowan, K. Cranmer, E. Gross and O. Vitells, *Asymptotic formulae for likelihood-based tests of new physics*, *Eur. Phys. J.* **C71** (2011) 1554, [1007.1727].
- [52] S. S. Wilks, *The Large-Sample Distribution of the Likelihood Ratio for Testing Composite Hypotheses*, *Annals Math. Statist.* **9** (1938) 60–62.
- [53] A. Wald, *An extension of Wilks' method for setting tolerance limits*, *Annals Math. Statist.* **14** (Mar., 1943) 45–55.
- [54] T. Junk, *Confidence level computation for combining searches with small statistics*, *Nucl. Instrum. Meth.* **A434** (1999) 435–443, [hep-ex/9902006].
- [55] A. L. Read, *Presentation of search results: The  $CL(s)$  technique*, *J. Phys.* **G28** (2002) 2693–2704.
- [56] CMS collaboration, V. Khachatryan et al., *Measurement of the double-differential inclusive jet cross section in proton-proton collisions at  $\sqrt{s} = 13\text{TeV}$* , 1605.04436.
- [57] T. Jacques, A. Katz, E. Morgante, D. Racco, M. Rameez and A. Riotto, *Complementarity of DM Searches in a Consistent Simplified Model: the Case of  $Z'$* , 1605.06513.

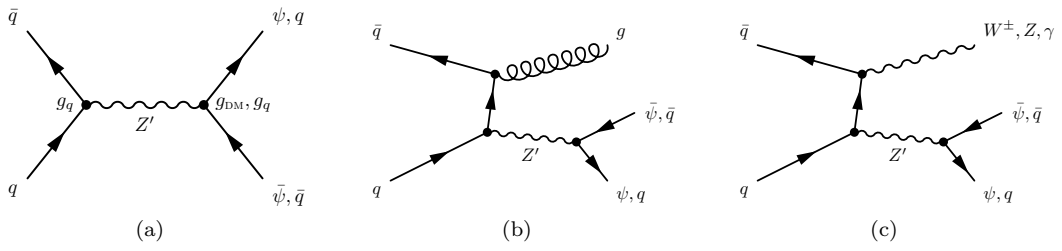


Figure 1: Relevant Feynman diagrams introduced by the simplified model at leading order. (a)  $s$ -channel production followed by decay to quarks or to DM, (b) associated jet production (c) associated gauge-boson production.

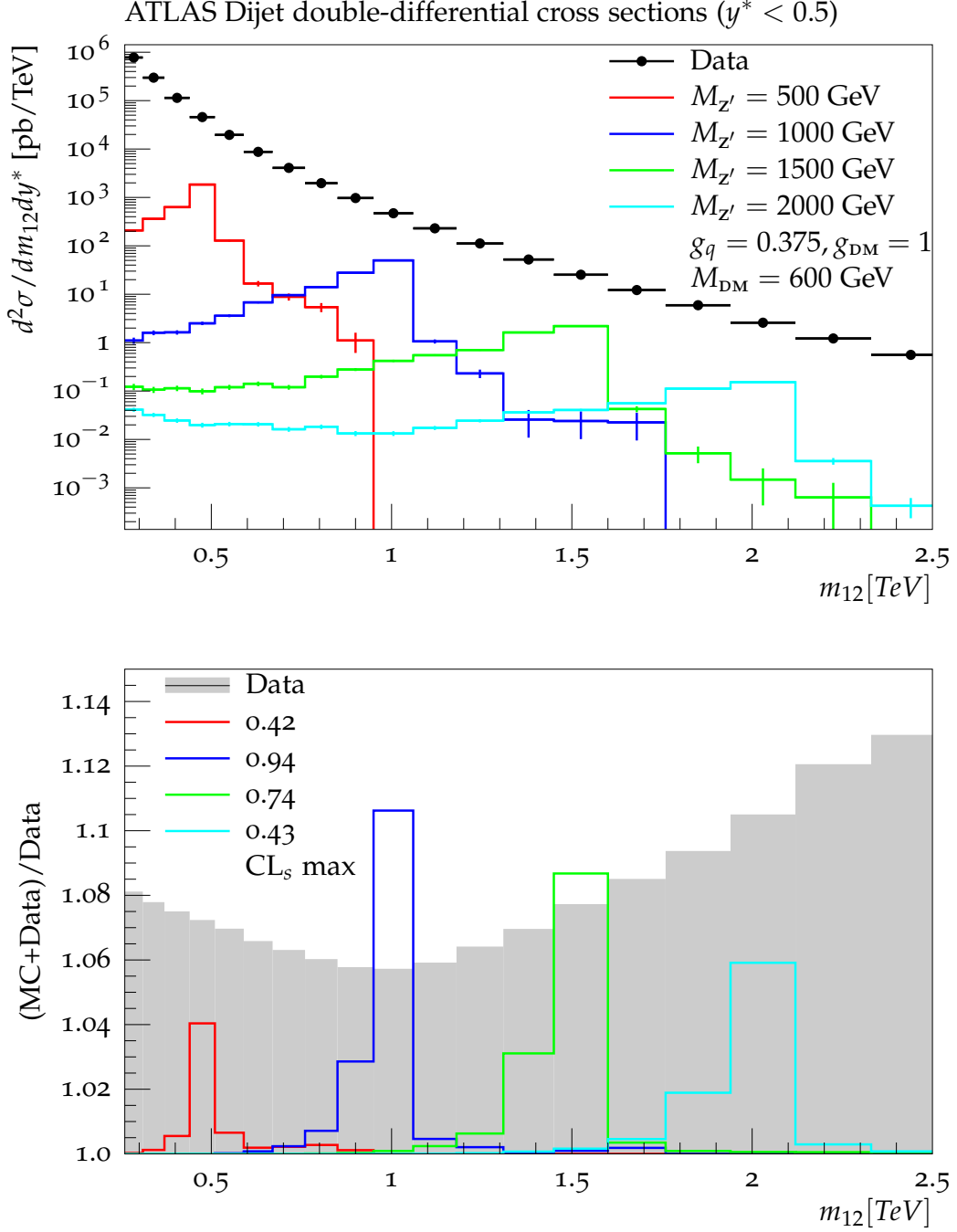


Figure 2: Outputs from Rivet for a measurement included in the limit setting process. Simulated signals for a sample of mediator masses are shown, superimposed on the double differential inclusive jet cross section in the most central rapidity region, binned by dijet mass and rapidity as measured by ATLAS at 7 TeV [31]. The upper plot compares the measured cross section to the model expectation, and the lower hand plot shows the perturbation in the ration compared to the relative uncertainty in the measurement. The signals form a 1D parameter space scan in mediator mass for fixed dark matter mass and mediator couplings;  $M_{DM} = 600$  GeV,  $g_q = 0.375$  and  $g_{DM} = 1$ . The corresponding exclusion limits are also given.

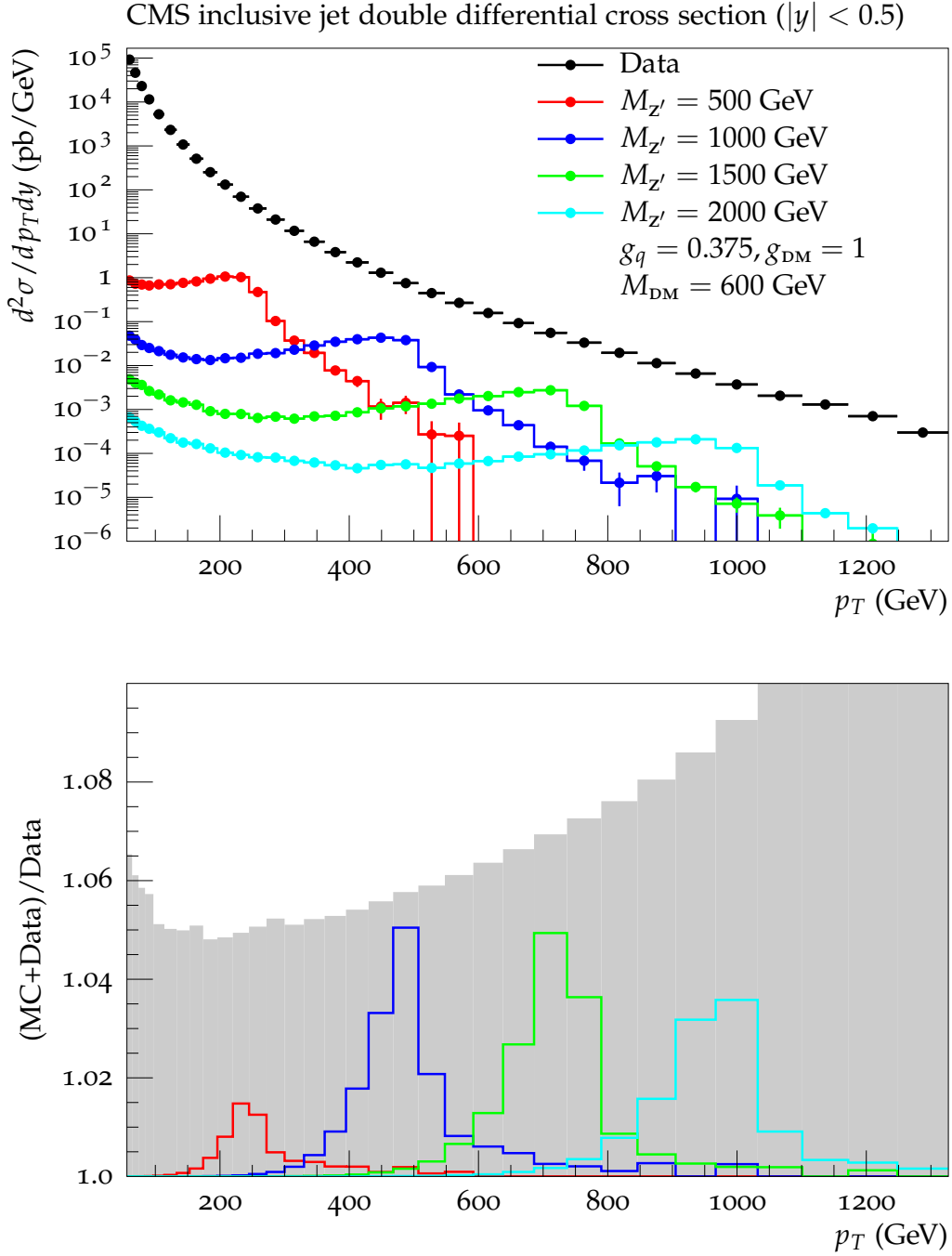


Figure 3: Outputs from Rivet for a measurement included in the limit setting process. Simulated signals for a sample of mediator masses are shown, superimposed on the double differential dijet cross section in the most central rapidity region, binned by leading jet  $p_T$  and rapidity as measured by CMS at 7 TeV [29]. The upper plot compares the measured cross section to the model expectation, and the lower plot shows the perturbation in the ratio compared to the relative uncertainty in the measurement. The signals form a 1D parameter space scan in mediator mass for fixed dark matter mass and mediator couplings;  $M_{\text{DM}} = 600$  GeV,  $g_q = 0.375$  and  $g_{\text{DM}} = 1$ .

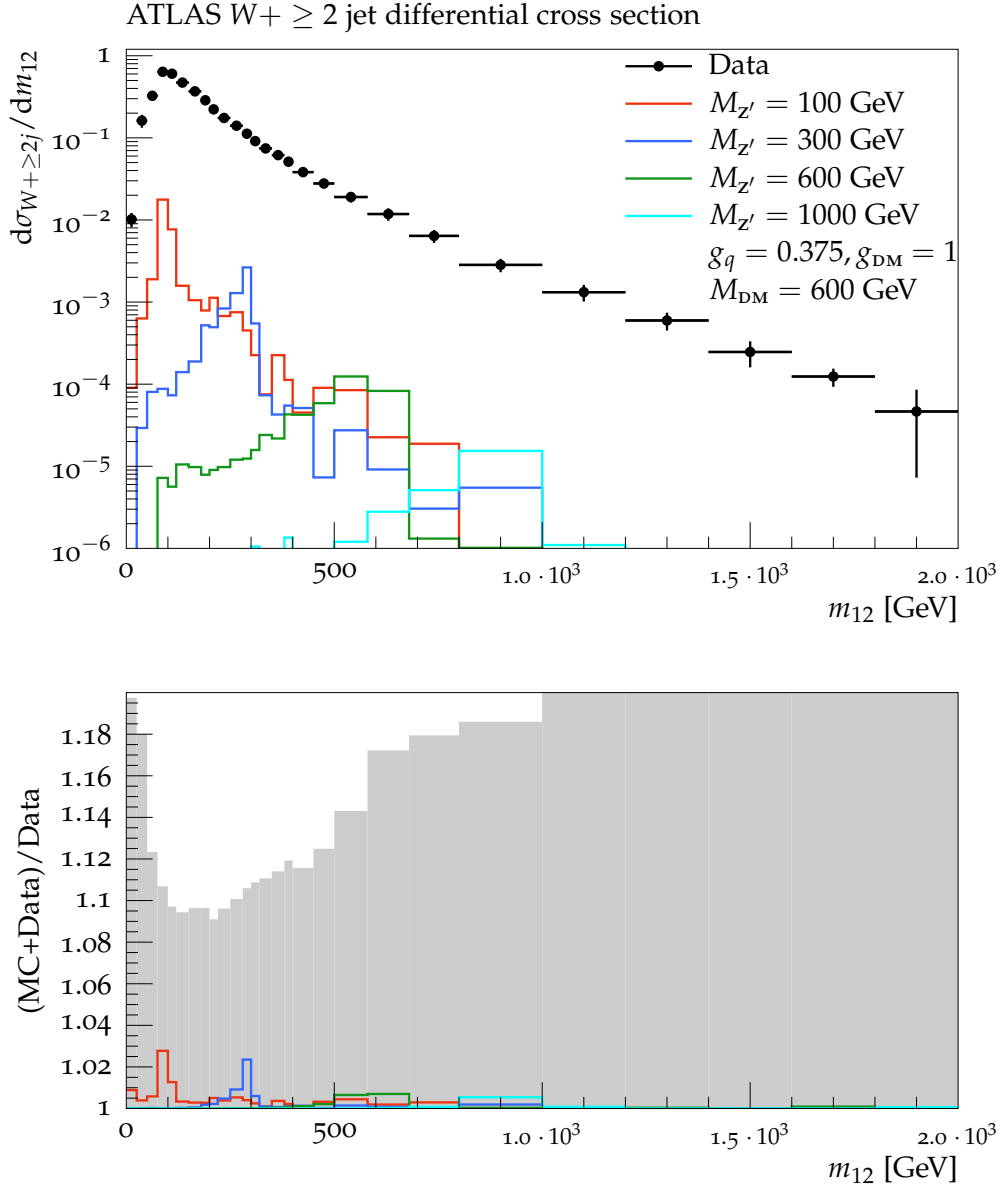


Figure 4: Outputs from Rivet for a measurement included in the limit setting process. Simulated signals for a sample of mediator masses, superimposed on the differential cross section for the  $W+ \geq 2$  jet process, binned in the mass of the dijet pair as measured by ATLAS at 7 TeV [35]. The signals form a 1D parameter space scan in mediator mass for fixed dark matter mass and mediator couplings;  $M_{DM} = 600$  GeV,  $g_q = 0.375$  and  $g_{DM} = 1$ .

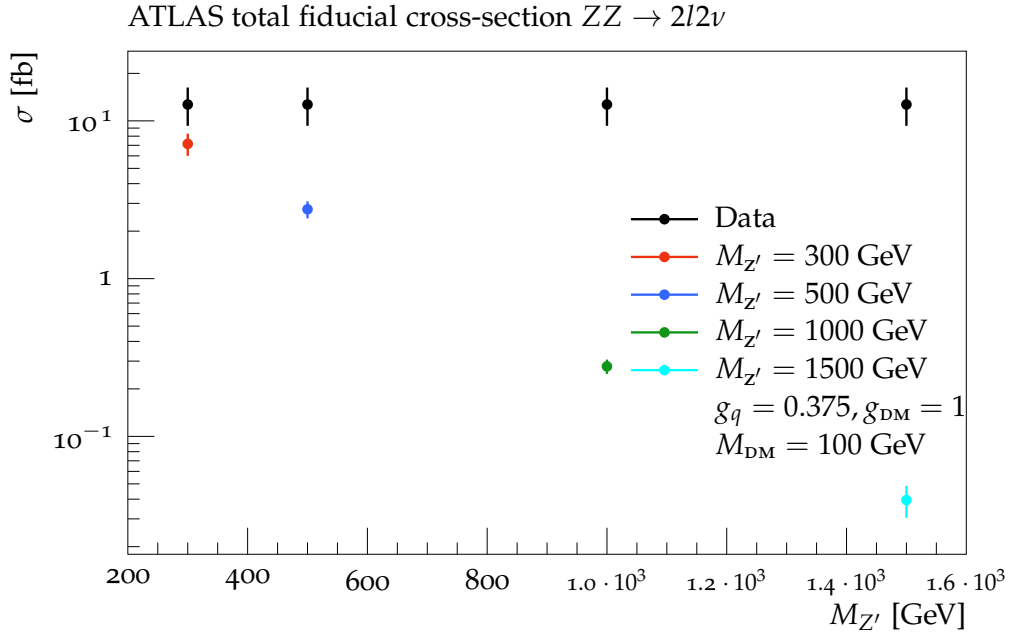


Figure 5: Outputs from Rivet for a potential measurement to be included in the limit setting process. Simulated signals for a sample of mediator masses, interpreted as perturbations to the  $ZZ \rightarrow l^+l^-E_T^{\text{miss}}$  cross section corresponding to the data as measured by ATLAS at 7 TeV [39]. The signals form a 1D parameter space scan in mediator mass  $M_{Z'}$  for fixed dark matter mass and mediator couplings;  $M_{\text{DM}} = 100$  GeV,  $g_q = 0.25$  and  $g_{\text{DM}} = 1$ .

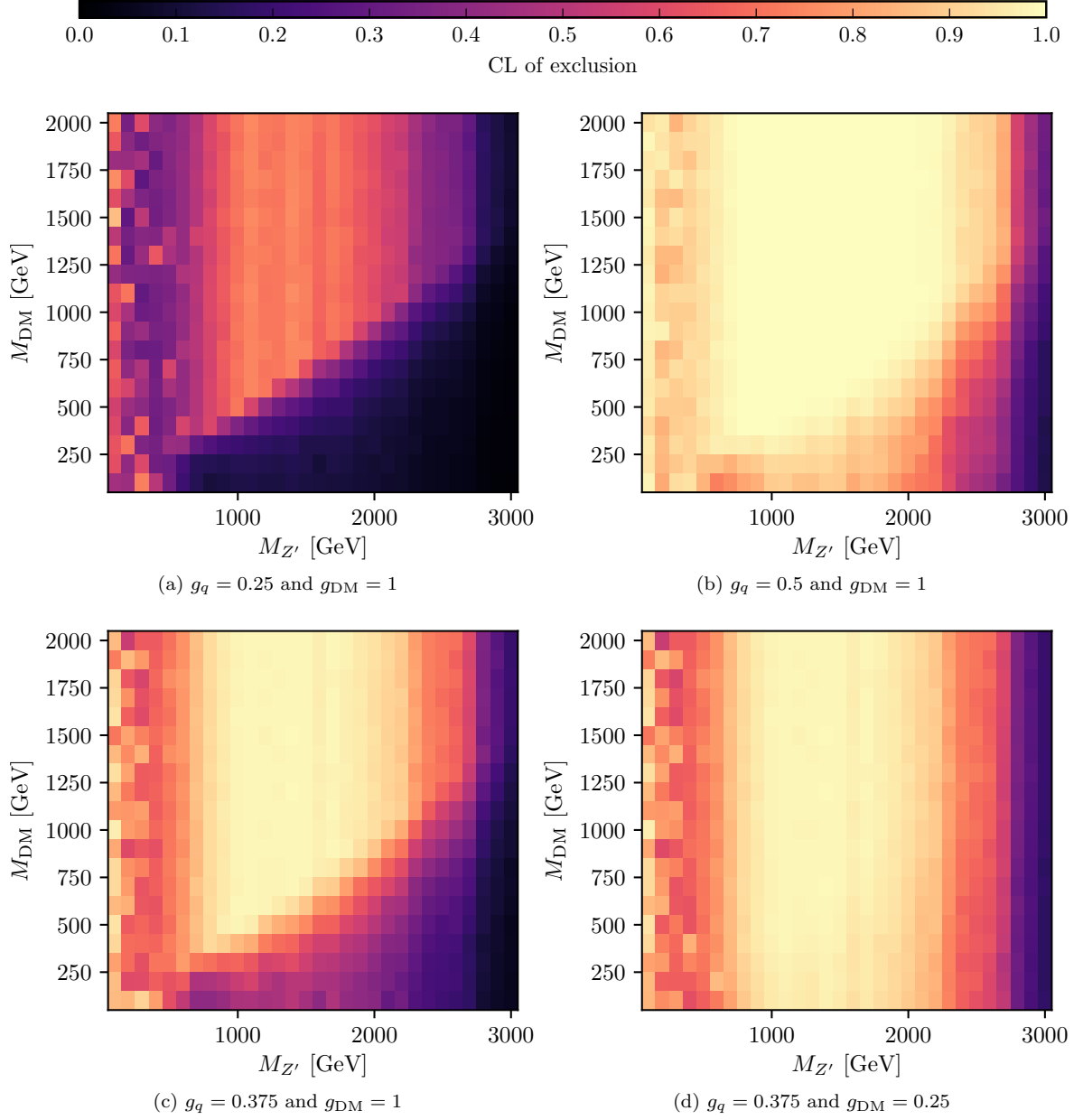


Figure 6: Heatmaps displaying 2D parameter space scans in fixed mass planes corresponding to a fixed  $g_{\text{DM}} = 1$  and variable  $g_q$ , with figure 6a representing  $g_q = 0.25$  and figure 6b representing  $g_q = 0.5$ . The confidence level of exclusion represented corresponds to testing the full signal strength hypothesis against the background-only hypothesis, calculated as outlined in section 4.3. The combination of measurements entering into the confidence level presented here is the maximally sensitive allowed grouping as outlined in section 4.2, considering all available measurements as listed in section 3. (a) Challenging scenario, (b) Optimistic (c) Intermediate (d) DM suppressed.

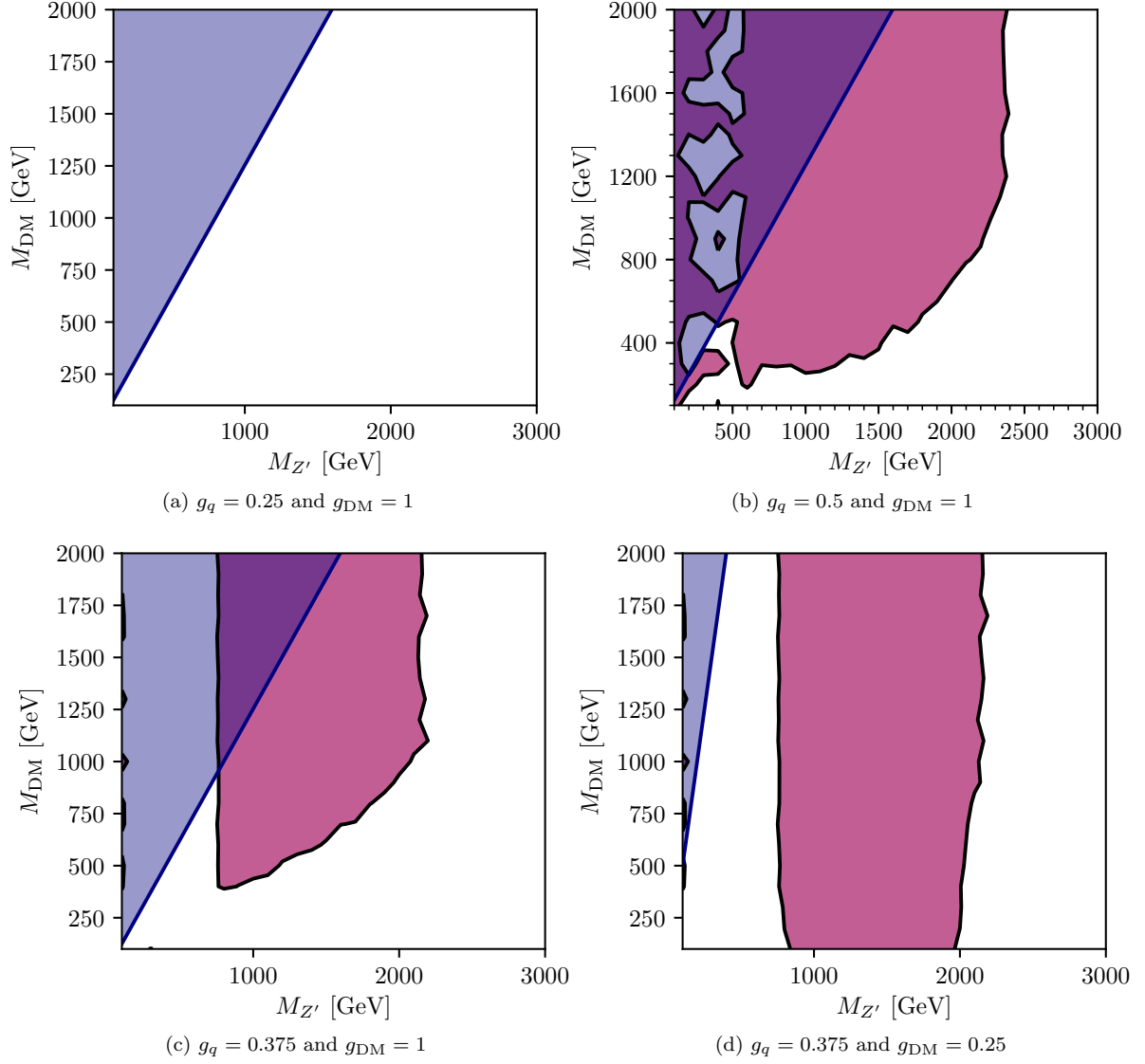


Figure 7: Contours in the  $M_{Z'}$  and  $M_{\text{DM}}$  plane for the considered values of  $g_{\text{DM}}$  and  $g_q$ , indicating the excluded region at 90% confidence level. The triangular shaded area is the region in which perturbative unitarity is violated by the model.